

Article

Arcing in Li-Ion Batteries

Theo Ledinski ¹, Andrey W. Golubkov ^{1,*}, Oskar Schweighofer ¹ and Simon Erker ^{2,*}

¹ Virtual Vehicle Research GmbH, 8010 Graz, Austria; theo@ledinski.at (T.L.)

² AVL List GmbH, 8020 Graz, Austria

* Correspondence: andrey.golubkov@v2c2.at (A.W.G.); simon.erker@avl.com (S.E.)

Abstract: Lithium-Ion battery cells and automotive battery systems are constantly improving as a result of the rising popularity of electric vehicles. With higher energy densities of the cells, the risks in case of failure rise as well. In the worst case, a fast exothermic reaction known as thermal runaway can occur. During thermal runaway, the cell can emit around 66% of its mass as gas and particles. An experimental setup was designed and showed that the gas-particle-vent of a cell going through thermal runaway can cause electric breakthroughs. These breakthroughs could start electric arcing in the battery system, which could lead to additional damages such as burning through the casing or igniting the vent gas, making the damage more severe and difficult to control. Uncontrollable battery fires must be prevented. The emitted gas was analyzed and the ejected particles were examined to discuss the potential causes of the breakthroughs.

Keywords: Li-ion battery; thermal runaway; safety; electric arcing

1. Introduction

Electric vehicle (EV) sales increased from 0.8 million in 2016 to 6.7 million over 5 years [1] and are expected to continue this upward trajectory. The energy density of Lithium-Ion battery packs has increased from 55 Wh L^{-1} to 450 Wh L^{-1} from 2008 to 2020. Together with their high specific energy values of up to 250 Wh kg^{-1} , it makes the Li-Ion batteries the most practical and commonly used batteries for modern EVs [2]. However, these properties bring a higher potential for damage in the event of battery failures, such as thermal runaway. Therefore, understanding the possible consequences is key for safety.

1.1. Battery Systems in Electric Vehicles

Battery systems in modern EVs vary from manufacturer to manufacturer, and this variation is partly due to the different cell types, which are explained in the subsequent section. A typical system for a pouch cell, such as the one used for the experiment, can be found in EVs produced in Germany. This system consists of a selectable number of battery modules, each containing 12 lithium-ion pouch cells. These modules are connected by a battery connector to form the battery system. Modern EV battery systems can have an energy storage of over 100 kWh. Such battery systems typically operate at a voltage of around 400 V, but systems of 800 V and above are becoming increasingly common. In the event of an electric arc in the system, the high voltage and low battery-pack resistance would lead to very high arc power and, therefore, to a high potential for damage.

1.2. Thermal Runaway of Li-Ion Cells

The high energy density of Li-Ion cells leads to higher risks in the case of failure. Overcharging, over-discharging, or internal short circuits can be the reasons for an increase in temperature well above manufacturer ratings. If a critical temperature is reached, a chain of exothermic reactions can be triggered. This will further increase the temperature, which accelerates the reaction. This mechanism of self accelerated degradation is known as thermal runaway. The thermal runaway can lead to temperatures up to 900°C . During



Citation: Ledinski, T.; Golubkov, A.W.; Schweighofer, O.; Erker, S. Arcing in Li-Ion Batteries. *Batteries* **2023**, *9*, 540. <https://doi.org/10.3390/batteries9110540>

Academic Editor: Pascal Venet

Received: 27 September 2023

Revised: 17 October 2023

Accepted: 25 October 2023

Published: 31 October 2023



Copyright: © 2023 by the authors. Licensee MDPI, Basel, Switzerland. This article is an open access article distributed under the terms and conditions of the Creative Commons Attribution (CC BY) license (<https://creativecommons.org/licenses/by/4.0/>).

this process, gas and particles are emitted by the cell. The state of charge of the cell has a significant impact on the reaction. A higher state of charge results in higher temperatures and greater gas emissions [3]. After the failure of the battery, but before the main thermal runaway, a smaller first venting may be observed. This happens due to electrolyte vaporizing and can be dangerous because the electrolyte is flammable and toxic. In the second and main venting, the particles emitted by an NMC cell are mainly composed of C, O, Al, Mn, and F. For a large part, lithium transition metal oxides $\text{Li}_x\text{M}_y\text{O}_4$ and transition metal oxides M_xO_y with M = CO; Ni Mn, for both cases, can be found [4,5]. The vented gas primarily consists of CO_2 , H_2 , CO and light alkanes (C_xH_y) [4,6].

1.3. Electric Arcing Inside a Battery Pack

Electric arcing is a phenomenon where an electric current flows through a gas-filled gap, creating a plasma channel that can reach very high temperatures and cause damage to the surrounding materials. Electric arcing can pose serious safety hazards for EVs, as it can burn through the battery housing and ignite flammable gases. Lai et al. stress that the electric arcs may destroy TR-propagation countermeasures in battery packs, and arc issues should be more emphasized in the future [7]. JRC reports TR-propagation tests on battery-pack level [8]. They found that the TR propagation pattern from cell to cell is non-sequential. They state that cells far from the initial TR position are triggered into TR by hot gases [8]. We propose a slightly different explanation; the initial cell releases hot vent-gas and particles, which could cause electric short circuits, arcing, and eventually the TR of cells which need not be adjacent to the initial cell.

The current and power of the electric arc depend on the arc resistance and the circuit impedance. The arc resistance is influenced by the arc temperature, length, diameter, and gas properties. In a theoretical battery pack with 66 A h-cells with a nominal voltage of 3.6 V and a resistance of 1 mΩ with 2p110s connection (2 cells in parallel and 110 cells in series), an estimation of the arcing current can be made. Doan [9] estimated that the maximum power of the arc P_{\max} is reached when the arc voltage is half of the system voltage V_{sys} , proposing the following Formula (1), which also includes the system resistance R_{sys} .

$$P_{\max} = (V_{\text{sys}}/2)^2 / R_{\text{sys}}; \quad (1)$$

with a system voltage of 396 V and a system resistance of 55 mΩ, the maximum power of the arc would be 712.8 kW. Compared to a typical electric welding machine with 10 kW, it becomes clear how dangerous such an arc could be. Because the maximum power method is rather conservative when estimating the power, a smaller theoretical battery pack was taken to compensate for that. With larger battery packs, powers of several MW could be reached.

Electric arcing can be initiated by electric breakdown or short circuit between two electrodes with a high voltage difference. Short circuits are recognized as the primary cause of thermal runaway. They are separated into internal short circuits in the battery cell and external short circuits of the electrodes outside the cell [10]. Abaza et al. [11] measured a peak current of 1850 A in an external short circuit of a 15 A h pouch cell. External short circuits lead to a significant increase in temperature that could pose additional risks, especially if the short circuit is initiated by the thermal runaway of another cell [10–13]. The electric breakdown, the other possible initiation mechanism for an arc, is explained in Section 1.4.

1.4. Electric Breakdown

An electric breakdown of a gas occurs when the voltage applied over a gas-filled gap is high enough to cause a multiplication of charge carriers due to various mechanisms. In this phenomenon, also known as arcing, the gas becomes conductive, resulting in a sudden drop of the gap voltage and a rise of the current flowing through the gap. When it is established, such an arc can be stable for as long as the external circuit is stable, but there needs to be an

initiation. An arc can be initiated by a short circuit of two separated electrodes induced by an external conductor connecting them for a moment. This mechanism works similarly to electric welding, where the electrode touches the working material and then is moved away to create an arc. Particles between two electrodes can become ionized and lead to an electric breakdown. The third possible mechanism is the breakdown of the gas without particles initiating it. Whether an electric breakdown of a gas can happen in a given setup depends on various factors, such as gas pressure, gas type, gap distance, voltage, and the electrodes in use. The breakdown voltage has proven to be a function of the combined parameter of gas pressure times gap distance $p \times d$. The gas dependent constants A and B can be calculated as shown in Equations (2) and (3), where σ_i is the electron impact ionization cross section, E_i is the ionization threshold, k_B is the Boltzmann constant, T is the temperature, and e is the elementary charge.

$$A = \frac{\sigma_i}{k_B \times T}, \quad (2)$$

$$B = \frac{\sigma_i \times E_i}{e \times k_B \times T}. \quad (3)$$

The third townsend coefficient or secondary electron emission coefficient γ describes the relation of electron emission to particles impacting a surface. It is dependent on the geometry of the electrodes and the ionization threshold of the gas. With the following Equation (4), known as the Paschen law, the breakdown voltage V_b can be calculated [14].

$$V_b = \frac{B \times p \times d}{\ln(A \times p \times d) - \ln[\ln(1 + 1/\gamma)]}. \quad (4)$$

1.5. Goals

The main goal of this work is to identify the root cause of electric breakthroughs in the airgap of electric components that might result in arcing in an automotive battery system. We investigated whether the venting gas or the ejected particles released from a battery cell in thermal runaway can cause such electric breakthroughs. Therefore we designed and performed an experiment, which is described in the next sections.

2. Materials and Methods

An experiment was designed in which the gas/particle jet from a cell in thermal runaway is funneled to go through the gap between two electrode-spheres. A sample holder with a vent opening facing two electrode-spheres was built using steel frames. It contained the cell, a heating element, and thermocouples. It was placed into a stainless steel reactor that was equipped with gas analyzers. An electric circuit was designed to measure the breakthrough characteristics inside the vent-gas-jet, also providing a triangle voltage with an amplitude of 400 V. The circuit was connected to the electrodes over the interface of the reactor. The cell was heated to start its thermal runaway. Measurements were conducted to see if electrical breakthrough events happen between the electrodes during thermal runaway. The ejected gas and particles are analyzed to discuss what the cause of potential breakthroughs could be. A sketch of the whole setup is shown in Figure 1. In the following subsections, the used components and methods are described in detail.

2.1. Used Li-Ion Cell

The cell used for the experiment is a 66 A h pouch cell made by a well-known cell producer of automotive Li-Ion cells, and can be seen in Figure 2. It was removed from an electric vehicle that was built in 2019. In the vehicle, the cell was part of a pack held together by the cyan-colored resin of which the remains are still visible. It had a mass of 893 g before the experiment. The main dimensions were a thickness of 11.7 mm, a width of 97 mm, and a length (without tabs and sealing) of 320 mm. The cell had a nominal voltage of 3.6 V with

an energy density of $\sim 270 \text{ Wh kg}^{-1}$. We assume that the cell has a graphite-based anode and an NMC cathode.

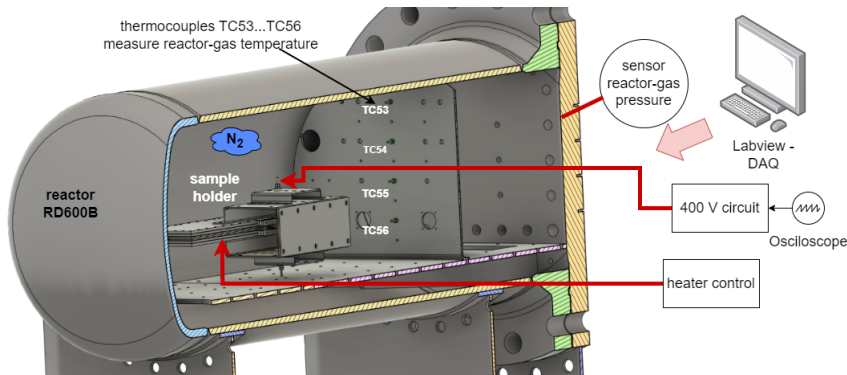


Figure 1. Overview of the whole test setup.

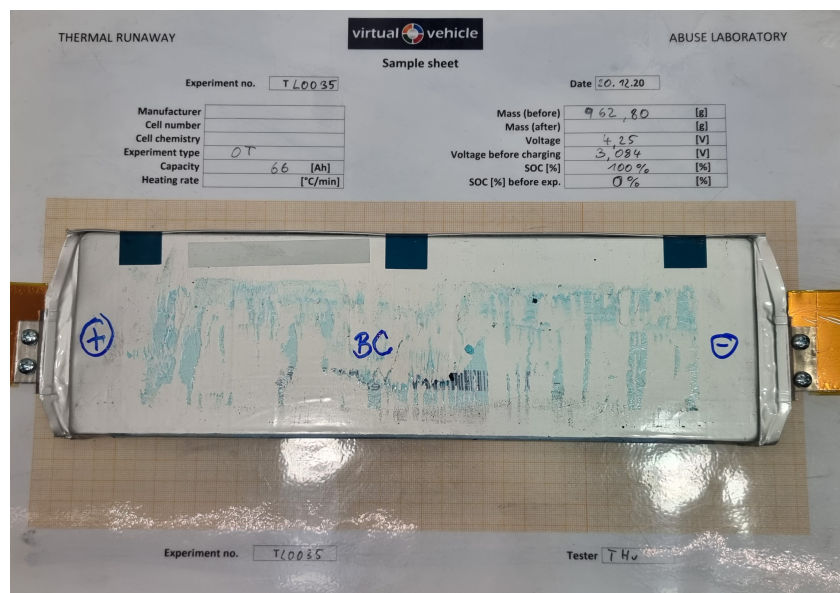


Figure 2. Tested cell sample. The blue plus and minus sign mark the cathode and anode.

2.2. Test Setup

A special sample holder was used, consisting of two steel-plates and several steel-frames and PTFE-frames. The PTFE frames were used as seals. The PTFE frames had cut-outs for the thermocouples, for the power lines of the heater and for the venting opening. The overall stack had only one opening for the venting with a cross section of

$$A_{vent} = 11 \text{ mm} \times 50 \text{ mm}. \quad (5)$$

Inside the stack thermocouples, TC10 … TC18 were integrated into a mica sheet to measure the temperature of the bottom cell-surface (Figure 3). Below the mica sheet containing the thermocouples there was an additional 5 mm layer of mica-sheets. Thermocouples TC1 … TC9 were inserted into the steel-spacer to measure the temperature of the top-surface (Figure 4). A heat-pad that covered the whole cell surface was on top of the steel-spacer. Steel was chosen for the spacer to conduct the heat from the heat-pad to the cell. Above the heat-pad a mica sheet with a silicon-foam tape-layer on top was used to compress the cell. The gaps between the sides of the cell with the terminals and the steel frame were filled with additional mica sheets to further funnel the gas through the venting opening. The individual layers are shown in Figure 5.

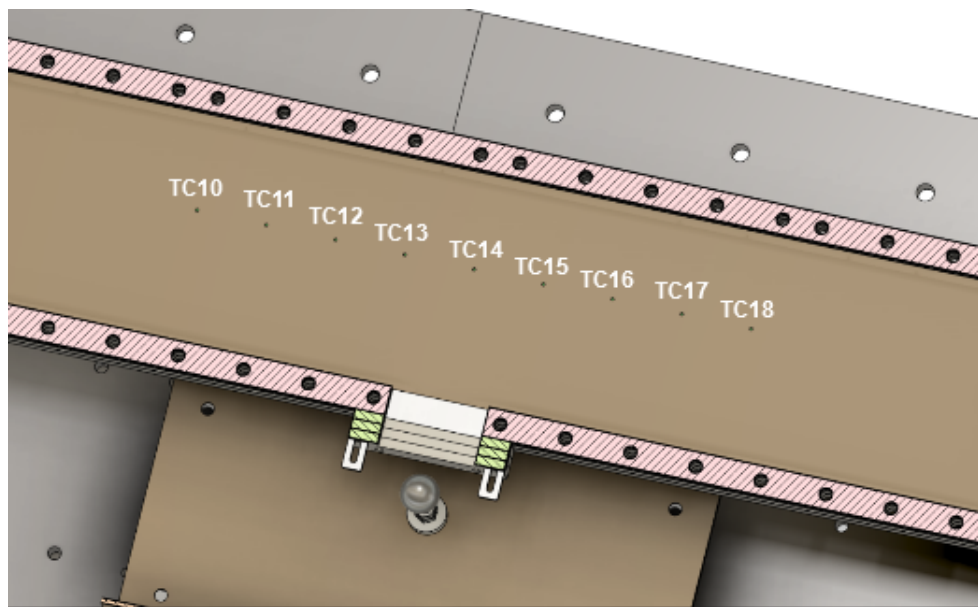


Figure 3. Position of the thermocouples below the cell in the mica sheet.

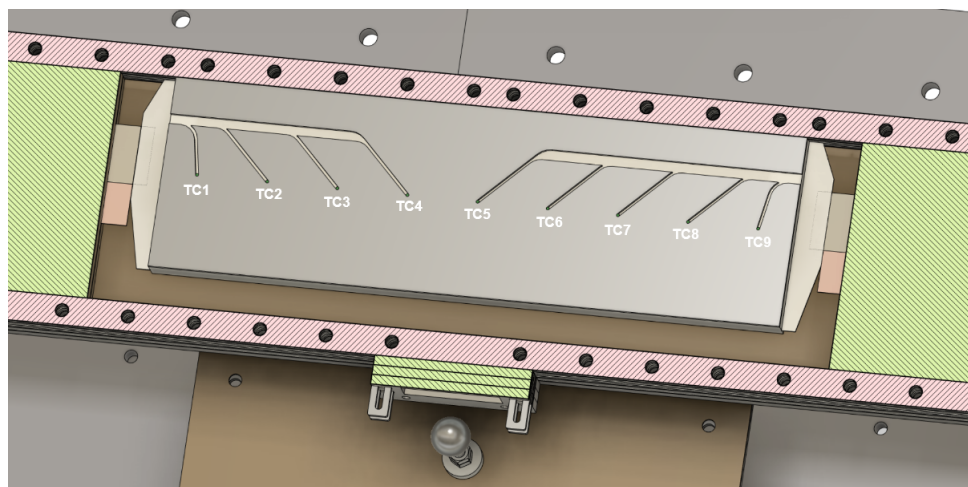


Figure 4. Position of the thermocouples above the cell in the steel-spacer.

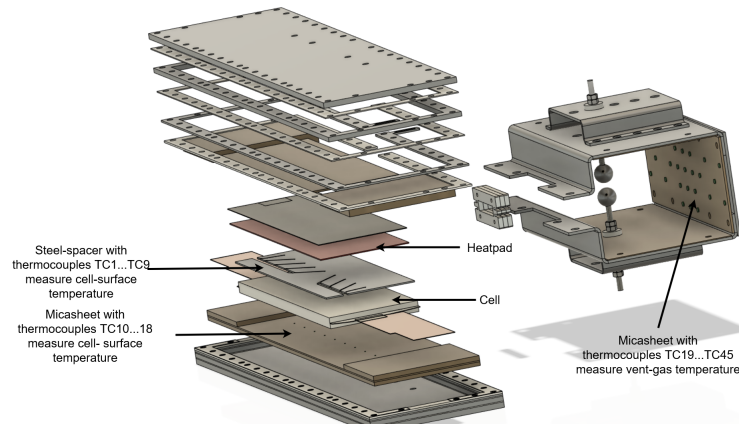


Figure 5. Exploded view of the CAD model showing the components and layers of the sample holder.

Opposite of the venting opening, in a distance of 121 mm, a venting target-plate was placed. Thermocouples (TC19 … TC45) were placed on the target-plate in a regular grid as shown in Figure 6. The cross section of the setup with the venting path is shown in Figure 7.

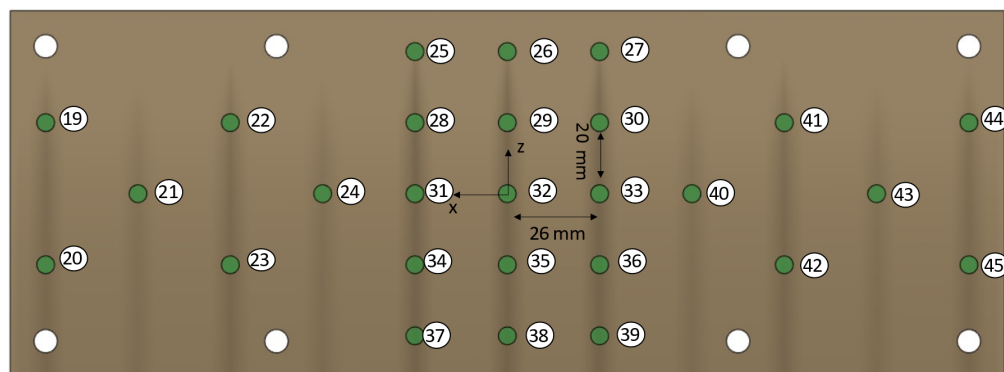


Figure 6. Position of the thermocouples (green circles) on the vent-gas target-plate.

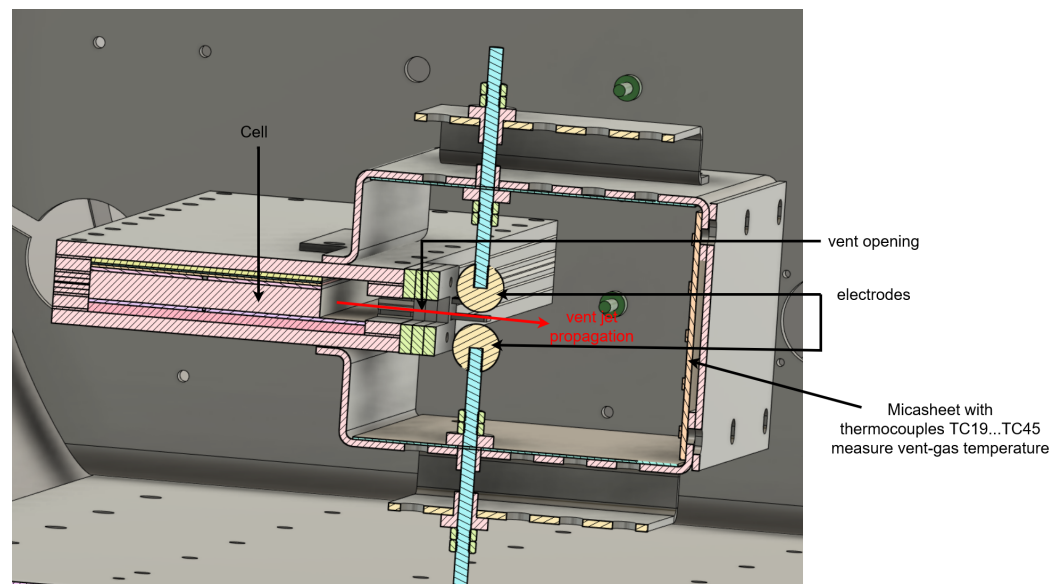


Figure 7. Cross section of the setup.

2.3. Reactor

The reactor RD600B (Custom made, Austria) that housed the test is made from stainless steel. It has a volume of 424.7 L and was built for pressures of up to 37 bar at up to 200 °C. The blind-flange was fixed and held all the interfaces for the thermocouples and electric connections. For the interfaces, there was a DAQ system in place that consisted of several components from Gantner Instruments GmbH. The main body could be slid open to access the stage for the sample holder. A sketch of the reactor is seen in Figure 8.

2.4. Gas Analysis

The gas composition in the reactor was measured with two different methods. To measure the permanent gases with gas chromatography there was a Inficon microGC Fusion 2-modul-system in place. The gas chromatograph was calibrated for H₂, O₂, N₂, CH₄, CO, CO₂, C₂H₆, C₂H₄ and C₂H₂.

To measure infrared active gases via Fourier transform infrared spectroscopy, there was a Bruker MATRIX-MG01 (Bruker Corporation, Billerica, MA, USA) with 0.5 wavenumber resolution in use. This measurement gave a higher accuracy for gases at low concentrations of only a few ppm.

2.5. Electric Circuit

A special isolated electric circuit was designed to measure the breakthrough characteristics inside the vent-gas-jet as shown in Figure 9. It consisted of a power supply that provided a triangle voltage with 5 Hz and a voltage amplitude of 400 V. Resistor R1 was used to discharge the internal capacitance of the power supply during negative flanks.

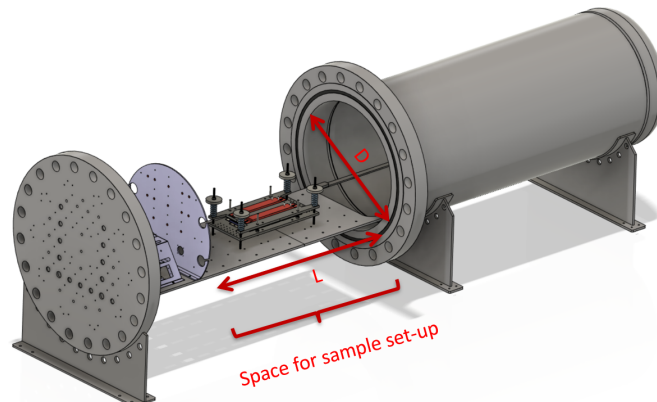


Figure 8. Three-dimensional (3D) sketch of the reactor. $L = 1000$ mm $D = 578$ mm.

Electrode current was measured by a voltage probe (Ch1) at the shunt R_{shunt} . As a safeguard, a current clamp was used to measure currents with a cut-off at 30 A. Electrode voltage was measured by the probe Ch2. The oscilloscope was set to 200 kS/s and the trigger was set on (Ch1) to detect discharge events.

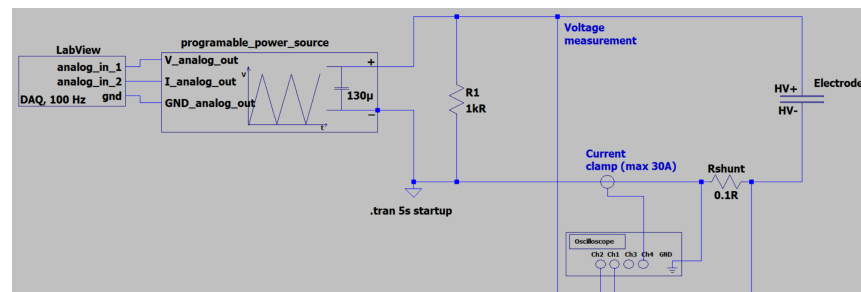


Figure 9. Electric setup to measure the vent-gas-jet characteristics.

In addition, the DAQ (Q-series X, Gantner Instruments, Schruns, Austria) (100 S/s) was connected to the analog outputs of the power supply, so that the internal current generation and voltage generation of the power supply could be monitored and synchronized with the TR of the cell. The analog outputs were only used for the synchronization. They are not accurate enough to analyse the actual discharge events.

For event analysis only, the measurement of the oscilloscope was used.

Used equipment:

- Oscilloscope Picoscope6402 (Pico Technology, Saint Neots, UK)
- Isolated programmable power supply: EA-PSI 95100-10 DT (EA Elektro-Automatik, Viersen, Germany) max 500 V, max 10 A;
- C1 capacitor (RS components, Gmünd, Austria) inside the power supply;
- R1 power resistors (RS components, Gmünd, Austria) 1 kΩ;
- R_{shunt} high quality shunt (Isabellenhuette Heusler, Dillenburg, Germany) with 0.1 Ω;
- Current clamp: Pico technology TA189 (Pico Technology, Saint Neots, UK) DC to 100 kHz Max 30 A. Overload 500 A, for 60 s.

The setup was tested by deliberately producing shorts between the electrode-spheres prior to the start of the experiment.

2.6. Experiment Method

The experiment method consisted of several subsequent steps. First, the cell was positioned in the sample holder cycled at normal conditions and charged to 100% state of charge. Then the reactor was closed, evacuated, and filled with nitrogen. The local heater was activated and the power source and oscilloscope were started, to measure the electric properties of the vent-gas-jet.

After the thermal runaway propagated through the whole cell, the gas composition was analysed. The reactor was evacuated to about 1 kPa absolute pressure and flushed with N₂ several times before it was opened to remove the cameras. Then the reactor was closed, heated up to 200 °C, and again evacuated to about 1 kPa absolute pressure and flushed with N₂ several times before it was opened again. Then, the dust and particles ejected by the cell were collected and sieved. The whole setup inside the reactor is shown in Figure 10.

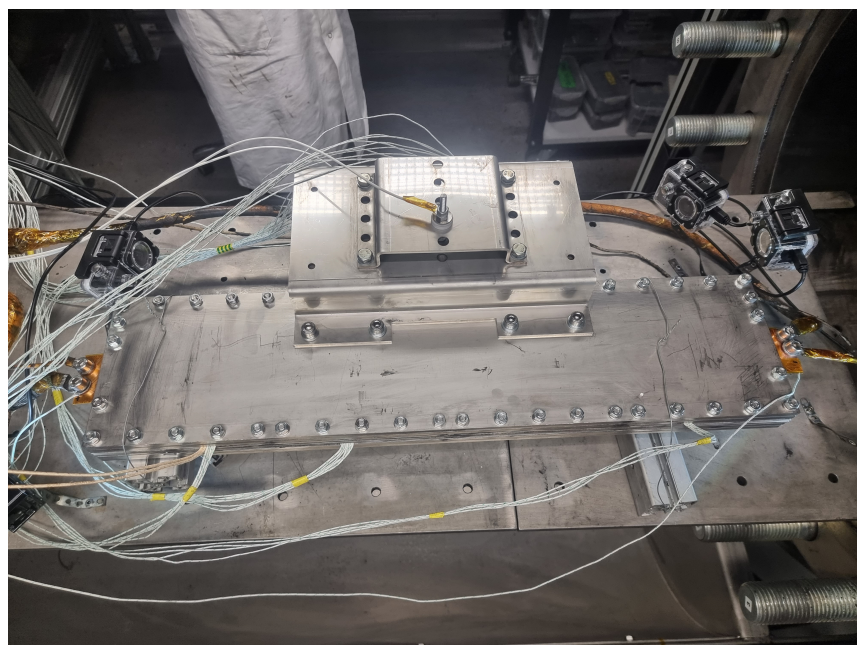


Figure 10. Complete setup inside the reactor.

3. Results

3.1. Cell Response

The cell went into thermal runaway 730.9 s after the heater was started. In the following Table 1, the notable events regarding the thermal runaway and the heat production are listed.

The measurements of all thermocouples are plotted in Figure 11. There, the moment of the thermal runaway and its consequences are clearly visible. Figure 12 shows the distribution of temperatures caused by the released hot gas and particles measured by the thermocouples with the arrangement shown in Figure 6. The heater was started 36.7 s after the experiment start and heated up until 780 s as seen in Figure 11. The thermal runaway of the cell starts at 767.6 s. The heater could have been turned off as soon as the thermal runaway started but the additional heat added by keeping it running did not change the result of the thermal reaction. The discharge events happened between 768 s and 770 s of the experiment. High temperatures were reached around the center of the vent-gas target-plate at x = 0 mm with some outliers at x = 52 mm. Highest vent-gas temperatures >1000 °C were measured by TK24 and TK34 at 772 s. After 800 s, the maximal average cell case temperature was reached and the cool down stage began.

The open reactor as well as the electrodes after the thermal runaway are shown in Figures 13–15. Compared to Figure 10, the large amount of particles all over the setup are

to be noticed. That dust was collected and examined later. Pictures showing the electrode gap before and during venting can be seen in Figure 16.

Table 1. Notable events. Here, t is the time and \bar{T}_{CC} is the average cell case temperature. U_C^* is the cell voltage at the start of the experiment.

t/s	$\bar{T}_{CC}/^\circ\text{C}$	Event
0	23	Start of Experiment
36.7	23	Cell heater ON, power >50 W
503.3	131	First cell case temperature (TK7) reaches >200 °C
766.6	171	1 s before start of 90% of the main gas release (immediately before start of TR).
767.6	171	Start of 90% of the main gas release (pressure starts to increase rapidly).
767.6	171	First vent gas temperature (TK34) reaches >200 °C
768.4	182	Arcing event 1
769.1	218	Arcing event 2 and 3
769.2	220	Arcing event 4 and 5
769.4	220	400 V power source switches off due to overload
770.9	218	First reactor gas temperature (TK56) reaches >200 °C
771.3	229	Voltage of the cell drops below 90 % of U_C^* .
772.1	247	Max. over-pressure (peak-baseline) inside the reactor $\Delta P_R = 1.4$ bar.
773.8	312	Voltage of the cell drops below 50 % of U_C^* .
775.1	378	Last cell case temperature (TK10) reaches >200 °C
794.2	539	Maximal local cell case temperature (TK5) $\hat{T}_{CC} = 681$ °C.
794.6	540	Cell heater OFF, power <50 W
800	547	Maximal average cell case temperature $\bar{T}_{CC} = 547$ °C.

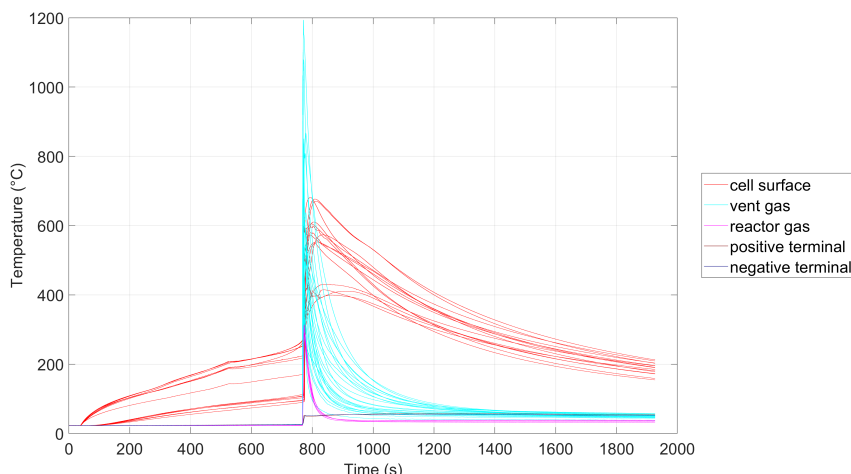


Figure 11. Temperatures of all sensors.

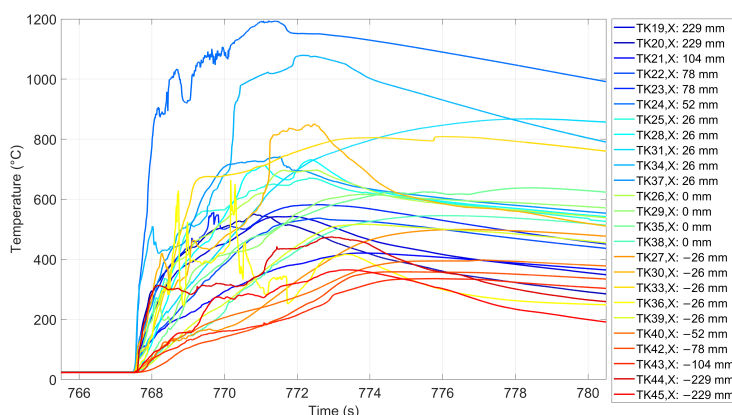


Figure 12. Temperature of the vent gas.

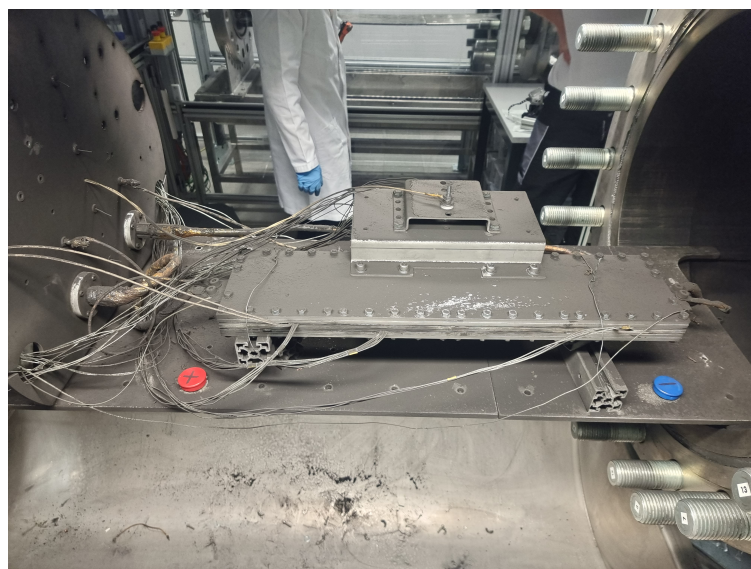


Figure 13. Setup inside the reactor after TR.



Figure 14. View of the electrodes after TR.

3.2. Gas Analysis

The amount of gas released by the cell during thermal runaway was calculated using the ideal gas equation and the measured values for gas temperature and pressure inside the reactor. Overall, 5.53 mol of gas was released as seen in Figure 17.



Figure 15. Removed electrodes. Even after shaking, some compressed dust remained sticking on the surface of the electrode-spheres covering the area which was hit by the vent-gas jet.

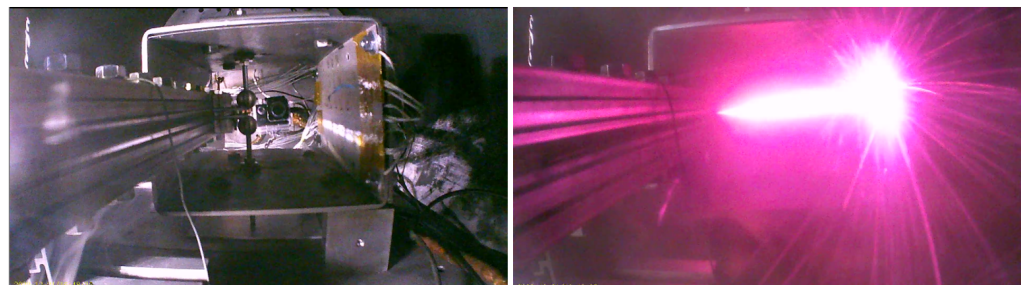


Figure 16. Video frame captions before (left) and during (right) the venting of the cell. The full videos are online at [15].

Gas component analysis of the main venting was performed about 10 min after the TR events of the cell. The measured components are shown in Figure 18. H₂, the component most favorable for arcing, made up 16% of the total gas released. CO₂ was the biggest component with 33%. The major chemical reactions during TR that are responsible for the released gas were discussed in a previous publication [16].

3.3. Electric Characteristics of the Vent-Gas-Jet

In Figure 19, the electrode voltage and current in comparison to the pressure in the reactor can be seen. Overall, five discharge events were detected, as seen in Figure 20. Discharge events happened at different voltage levels and at both the rising and the falling voltage flanks. In Figure 21, the first event is shown. It happened on the rising flank at 276 V. Events 2 and 3 both happened in a time span of 7 ms on the falling flank at about 280 V and 260 V as seen in Figure 22. Events 4 and 5 happened over the voltage peak, and event 5 started before the voltage could go all the way back up to its supposed value after event 4 as seen in Figure 23. Unfortunately, after the 5th discharge event, the power supply turned itself off due to over-power-protection, so further possible events could not happen even though the reaction was still going on as seen in the pressure in Figure 19.

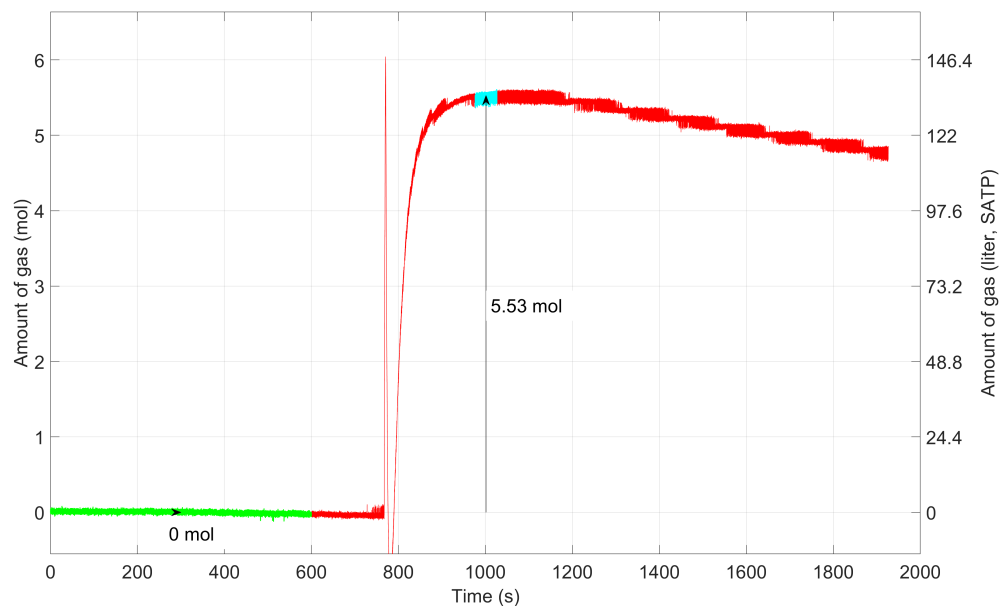


Figure 17. Amount of gas n in the reactor. Timespan annotated in green is the timespan before thermal runaway; here n -baseline is set as zero. Timespan annotated in cyan is the timespan after thermal runaway where gas is assumed to be in equilibrium. The released amount of gas is annotated with the arrow.

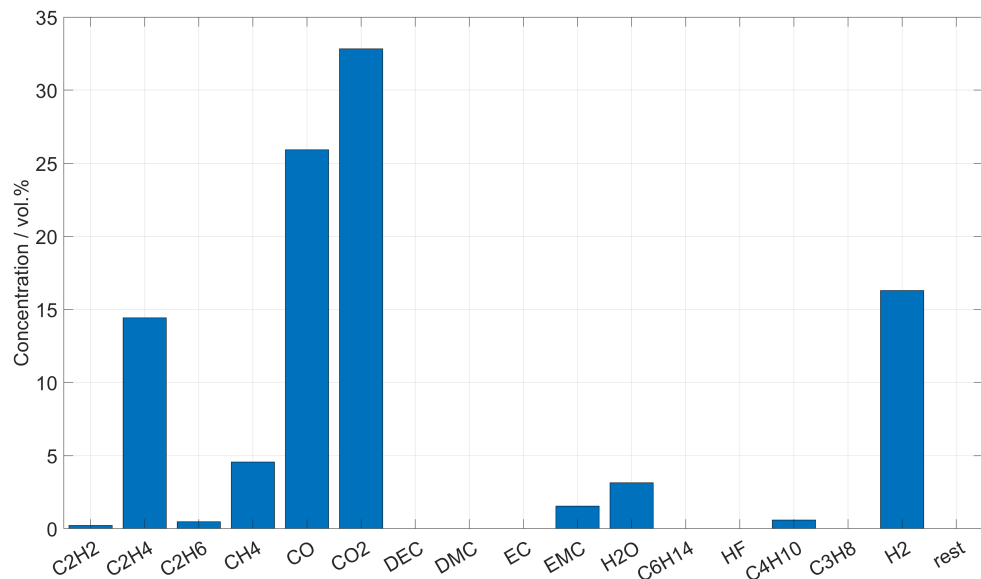


Figure 18. Composition of the gas which was released by the cell.

3.4. Cell and Ejected Material after Thermal Runaway

The cell went through thermal runaway, resulting in the ejection of a big part of its mass in particles and gas. The remains of the cell were extracted. The cell mass changed by -66.1% from 962.80 g to 326.80 g. Figure 24 shows the cell after the experiment.

Fine particles and copper pieces were released by the cell as seen in Figure 25.

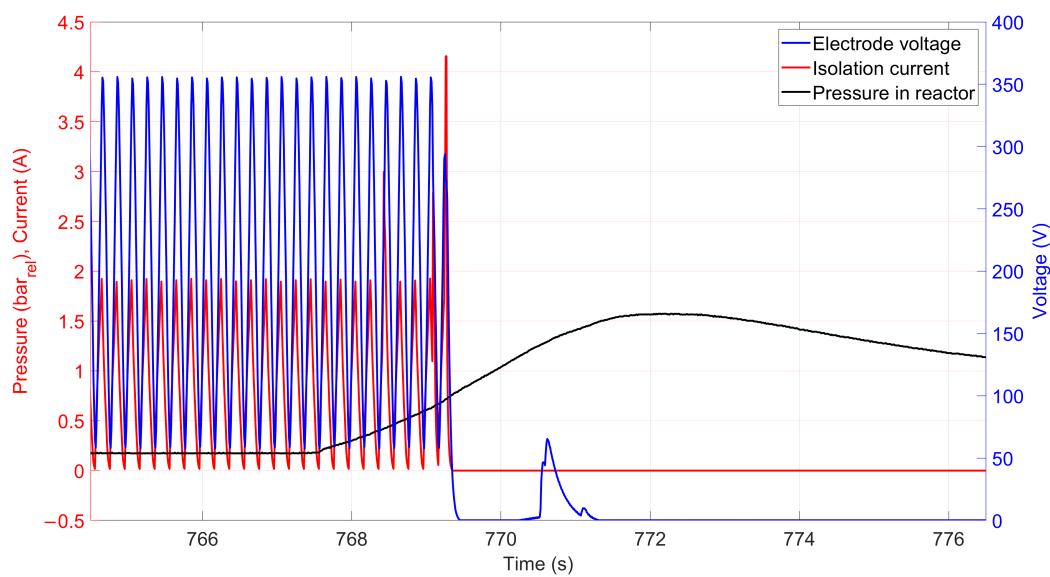


Figure 19. Comparing analog outputs of the power source for electrode voltage and current to the pressure in the reactor. (Note that the analog outputs of the power source could not keep up with the fast signal change, therefore they peak at merely 350 V instead of the real value of 400 V).

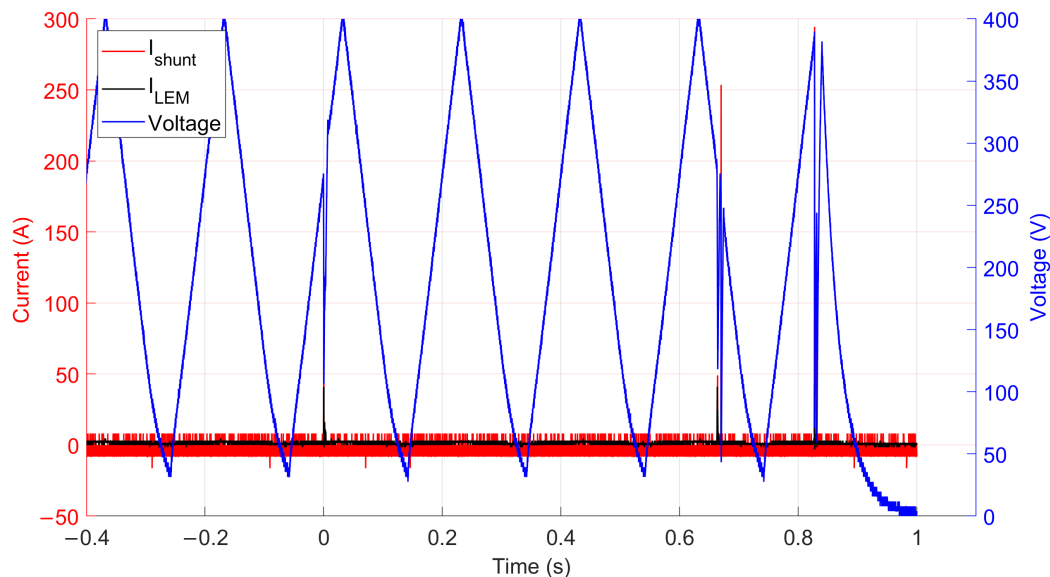


Figure 20. Oscilloscope measurement of voltage and current showing all breakthrough events. (The oscilloscope time is referenced to the first trigger).

After the sieving of 135.40 g of ejected material, the following copper pieces were found:

- 14 pieces >10 mm;
- 46 pieces 5 mm to 10 mm;
- 48 pieces <5 mm.

Overall, 60 significant pieces were found that could have shortened the two electrodes. The copper pieces can be seen in Figure 26.

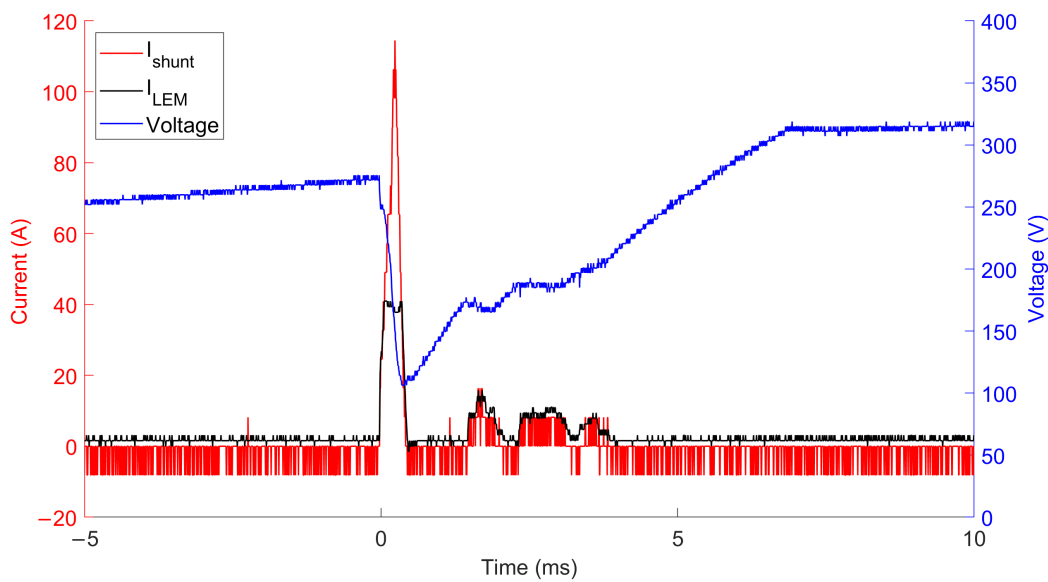


Figure 21. Oscilloscopemeasurement of voltage and current during breakthrough event 1.

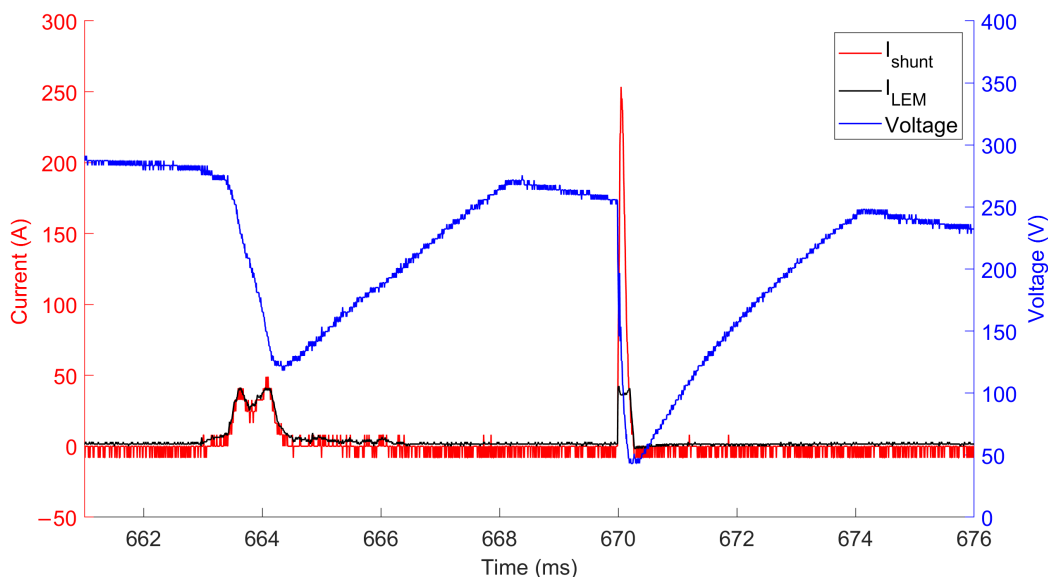


Figure 22. Oscilloscopemeasurement of voltage and current during breakthrough events 2 and 3.

The sieved dust was compressed and its resistance measured at a voltage of 20 V, as seen in Appendix A. The results are shown in Figure 27. The sieved dust still contained copper pieces that are responsible for a drop in resistance. In the more finely sieved dust, the number of copper pieces and therefore the measured resistance varies. The dust in V2 seemed to have less copper in it than V3, which explains the different curve compared to the other results. This implies that the actual resistance of the dust without any copper particles would be much higher.

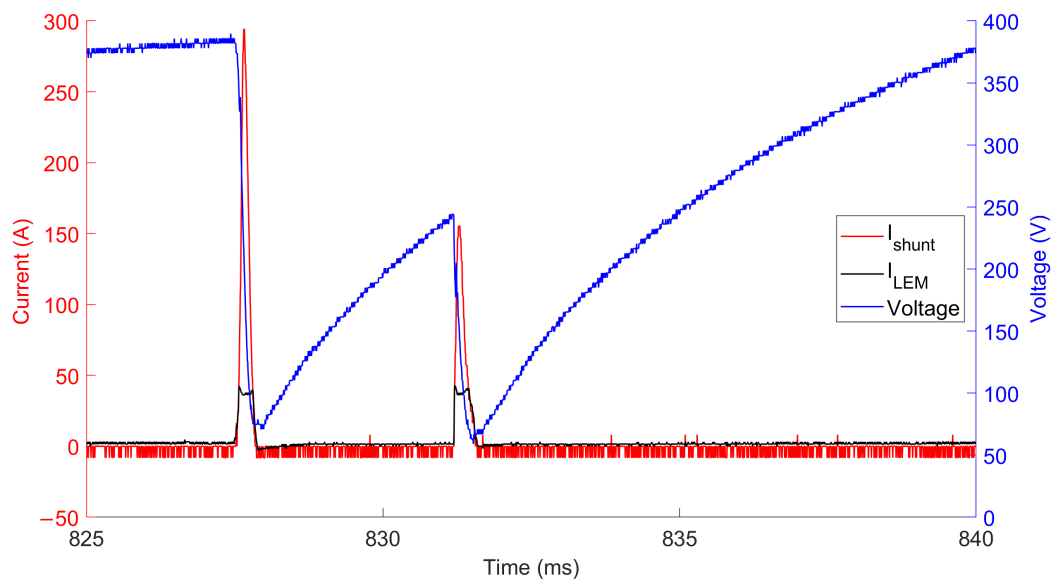


Figure 23. Oscilloscopemeasurement of voltage and current during breakthrough events 4 and 5.



Figure 24. Cell after the TR.



Figure 25. Copper pieces lying around the sample holder.

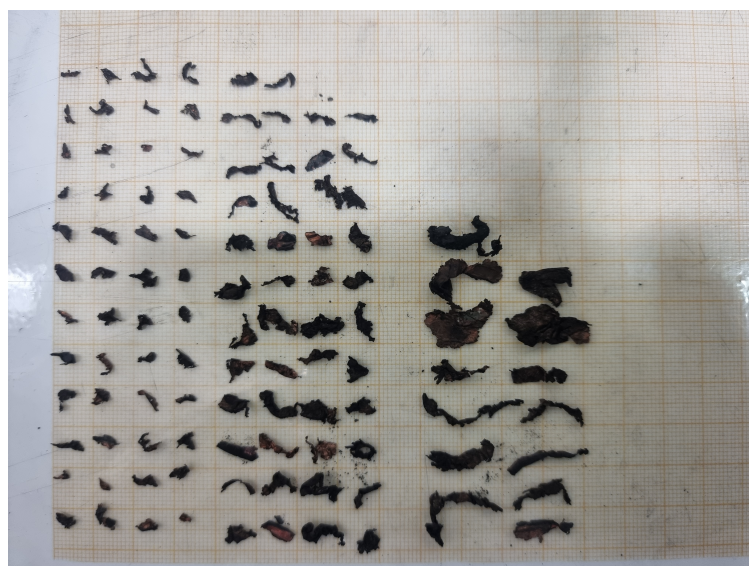


Figure 26. Sieved copper pieces.

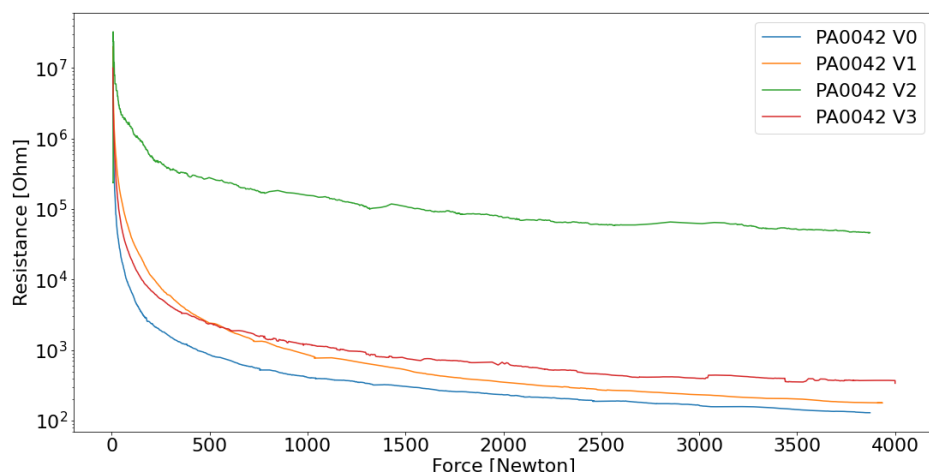


Figure 27. Force over resistance of the dust. V0 and V1 are sieved with 2.8 mm and V2 and V3 with 1 mm.

4. Discussion

It is clear that the gas-particle-vent of the cell going through thermal runaway is the reason for the electric breakthrough events. But, as described above, there are three major components of the vent corresponding to three possible mechanisms that could explain the measured events. First, there could be arcing through the gas due to a changed composition and pressure. Secondly, there could be electric conduction by the particle conglomerate passing by and touching the electrodes. The third possible explanation would be the larger copper pieces touching both electrodes while passing through. In the following subsections, all mechanisms and their likelihoods are discussed. In Figure 28, the possible mechanisms are schematically illustrated.

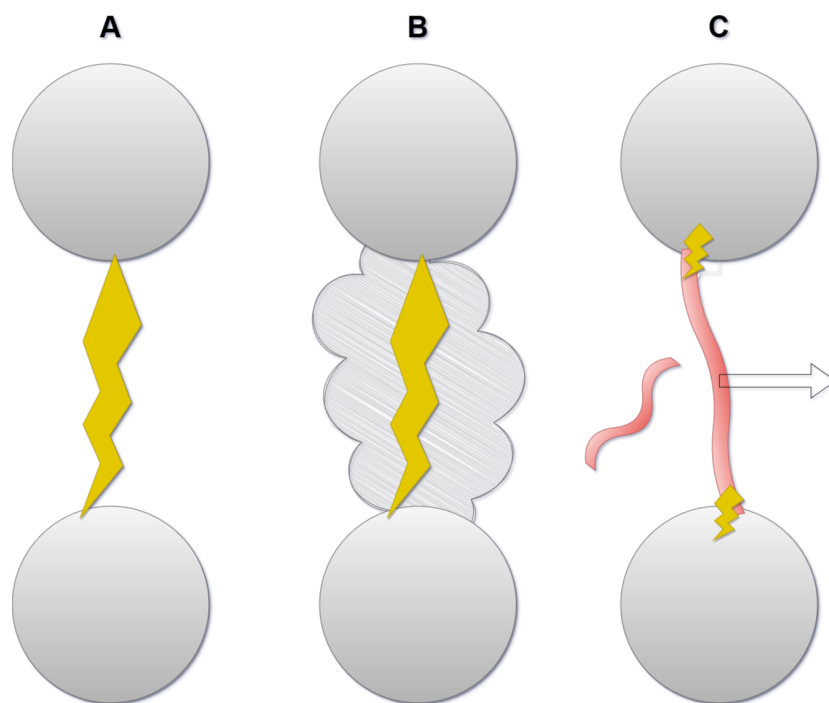


Figure 28. Schematic illustration of the possible breakthrough mechanisms. (A) Arcing through gas, (B) Breakthrough due to dust, (C) Copper piece connecting the electrodes.

4.1. Arcing through Gas

To see if arcing through the gas is an optional explanation for the measured breakthrough events, an approximation using the Paschen law Equation (4) was made. The impact of the gas temperature on the breakthrough voltage in a gas mixture is primarily given by the change of gas composition with changing temperatures [17]. Since our approximation was made for the component with the lowest breakthrough voltage, the temperature has no significant effect on the result. Out of the gas components analysed, H₂ would give the lowest breakthrough voltage with its values of $A = 3.83 / (\text{Pa}/\text{m})$ and $B = 104.1 / (\text{Pa}/\text{m})$ [18]. The values of the pressure and the gap are taken as $p = 1.2 \text{ bar}$ and $d = 5 / (\text{mm})$ to give the smallest $p \times d$ value. With the approximation $\gamma = 0.1$ for the secondary electron emission coefficient, this results in a minimal breakthrough voltage of $V_b = 9098 \text{ V}$. This shows that, even with the most favorable assumptions made, arcing through the gas is still not possible in our setup with max 400 V.

Additionally, there seemed to be no correlation between the voltage and the occurrence of the events. Events happened at the rising and the falling flanks at different voltage values between 250 V and 400 V. If the increased electric-field was the reason for the breakthroughs, then we would expect electric breakdown during the rising flank above some voltage threshold. This was not the case in the experiment.

In a study about the dielectric breakdown strength of vented Li-Ion electrolyte, Nybeck et al. [19] came to the conclusion that the vented gases maintain a similar dielectric strength to ambient air.

4.2. Dust as Arcing Starter

Consequently, the ejected material has to be the reason for the measured breakthroughs. No applicable literature was found on the effect of similar amounts of dust on the breakthrough voltage. To give a worst-case estimate, the resistivity at the maximum mechanical compression applied to the dust as seen in Figure 27 was calculated using Equation (A1). An applied force of 3.8 kN in the test setup shown in Figure A2 equals a dust compressed by 1.96 MPa. The first 45° of the electrode sphere were covered in compressed dust after the experiment (Figure 15). Therefore, the cross section of the spheres at 45° with an area of $A = 50 \text{ mm}^2$ and the distance of the middle points between the poles and the cross sections $L = 7.93 \text{ mm}$ have been taken, along with the calculated resistivity, to compute an estimate for the resistance of the dust between the electrodes. The resistivity and resistance between the electrodes for each dust sample are shown in the following Table 2.

Table 2. The calculated resistivity and corresponding resistance between the electrodes of the 4 dust samples which were compressed with 1.96 MPa.

Sample	$\rho / \Omega \text{mm}$	R / Ω
V0	39.67	6.29
V1	54.46	8.64
V2	14,272.15	2263.56
V2	111.66	17.71

This shows that the ejected compressed dust copper conglomerate could result in low enough resistances to cause breakthrough. Whether the arcing was caused by the conglomerate or by larger single copper pieces could not be determined by this experiment, but it gives indicatives.

4.3. Copper Pieces as Arcing Starter

Large single copper pieces big enough to be in contact with both electrodes at the same time could be the cause of the breakthrough events. During thermal runaway, the cell ejected $\sim 636 \text{ g}$. When 135.40 g already contained 60 copper pieces with $>5 \text{ mm}$, then $\sim 636 \text{ g}$ could contain up to 281 such pieces. The significant number of potentially released copper pieces could cause the discharge events between the electrode-spheres. Most of the pieces have the right size in only one possible orientation, therefore most of them would fly through the gap without causing a discharge, which would explain why more events were not seen.

5. Conclusions

The cell was put into a sample holder with an opening that funneled the gas-particle-vent between two sphere electrodes. This setup was put into a stainless steel reactor and the electrodes were connected to a power supply applying a triangle voltage with an amplitude of 400 V and an electric measurement setup to detect electric breakthroughs. The cell was heated until it went through a thermal runaway. Five discharge events were measured during the ejection of gas and particles.

The cell went into thermal runaway 730.9 s after the heater was started and produced 5.53 mol of gas during the thermal runaway. $\sim 636 \text{ g}$ of mass was ejected. 135.40 g of that mass was examined and 60 copper pieces with $>5 \text{ mm}$ were found. We clearly identified the particles ejected by the cell during thermal runaway to be the root cause of electric breakthroughs. Venting gas alone could not explain the measured breakthroughs in our

test setup. The ejected copper could have caused the five measured discharge events either as a conglomerate of smaller pieces or as single larger pieces.

If a cell of a battery system inside an electric vehicle goes into thermal runaway and the vent gas jet wears off isolation material due to abrasion and high temperatures, arcing could happen and cause further damage. Thus, arcing poses a risk worth taking into consideration during the design of safe battery systems. It is recommended to consider the direction of the vent jet in the case of a thermal runaway and make sure it does not face electric connections where it could lead to breakthroughs and arcing.

Many questions regarding the influence of venting and particles on the possibility of arcing are still unanswered. The authors are currently working on follow-up projects to better understand the conditions that may cause electric breakthroughs in battery packs. This includes influences of cell-types, electrode geometries, electrode voltages, and particle deposition. Further research could include the influence of the state of charge and experiments under ambient atmosphere conditions.

Author Contributions: Conceptualization, A.W.G. and S.E.; Investigation, T.L. and O.S.; writing—original draft preparation, T.L. and A.W.G. All authors have read and agreed to the published version of the manuscript.

Funding: The project was funded by the program “Mobilität der Zukunft” of the Austrian Ministry of Climate Action, Environment, Energy, Mobility, Innovation and Technology (BMK). The publication was written at Virtual Vehicle Research GmbH in Graz and partially funded within the COMET K2 Competence Centers for Excellent Technologies from the Austrian Ministry of Climate Action, Environment, Energy, Mobility, Innovation and Technology (BMK), the Austrian Federal Ministry for Digital and Economic Affairs (BMDW), the Province of Styria and the Styrian Business Promotion Agency (SFG). The Austrian Research Promotion Agency (FFG) has been authorised for the programme management. Additional funding and material was provided by AVL List GmbH.

Data Availability Statement: Raw data and the videos of the experiment are provided online at <https://repository.tugraz.at/records/wt2bh-20214> (accessed on 24 October 2023).

Conflicts of Interest: The authors declare that they have no known competing financial interests or personal relationships that could have appeared to influence the work reported in this paper. Simon Erker is employee of AVL List GmbH, who provided funding and technical support for the work. The funder had no role in the design of the study; in the collection, analysis, or interpretation of data, in the writing of the manuscript, or in the decision to publish the results.

Abbreviations

The following abbreviations are used in this manuscript:

EV	Electric vehicle
BMS	Battery management system
TR	Thermal runaway
TC	Thermocouple
PTFE	Polytetrafluoroethylene
DAQ	Data acquisition system

Appendix A. Dust Resistivity Measurement

For the resistivity measurement of the dust a non conductive calcium silicate cage, that is open on the top and closed with a mica sheet on the bottom, was taken. Through two openings on opposing sides copper electrodes were inserted. The cage got filled up to the top with dust and closed with a mica sheet. This setup is shown in Figure A1 as a schematic and in Figure A2 by a picture. The sides of the dust volume both measured 44 mm and the copper electrodes rose 0.3 mm above the ceramic plate.

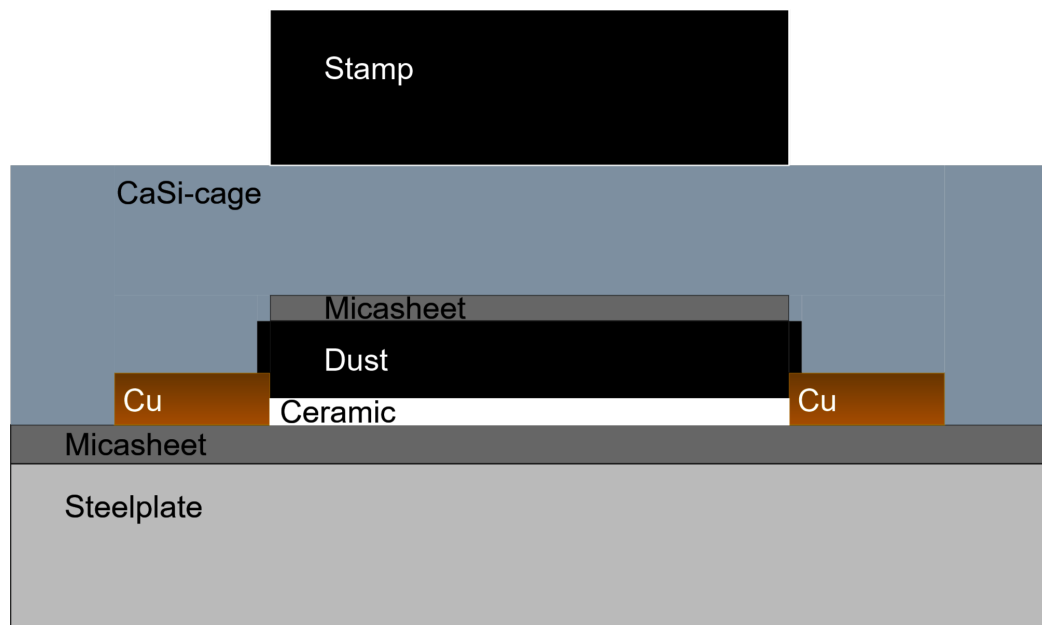


Figure A1. Schematic of the dust resistivity measurement.

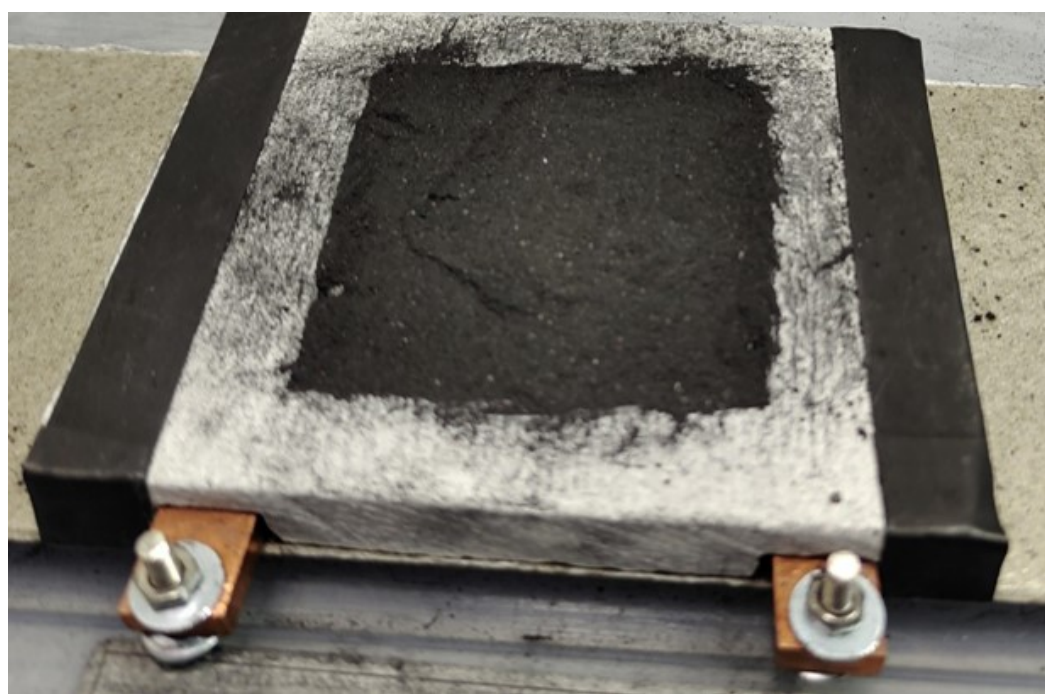


Figure A2. Picture of the dust in the measurement setup.

A 20 V voltage was applied while the dust got slowly mechanically compressed. The power supply was set to a maximal power of 40 W and 2 A. With the exact voltage and current the resistance could be calculated. With the resistance R , the distance between the electrodes L and the surface area of the electrodes A the resistivity ρ could be calculated by the following Equation (A1).

$$\rho = \frac{A \times R}{L}. \quad (\text{A1})$$

References

1. IEA. Global Sales and Sales Market Share of Electric Cars, 2010–2021. Available online: <https://www.iea.org/data-and-statistics/charts/global-sales-and-sales-market-share-of-electric-cars-2010-2021> (accessed on 24 October 2023).

2. Muralidharan, N.; Self, E.C.; Dixit, M.; Du, Z.; Essehli, R.; Amin, R.; Nanda, J.; Belharouak, I. Next-Generation Cobalt-Free Cathodes—A Prospective Solution to the Battery Industry’s Cobalt Problem. *Adv. Energy Mater.* **2022**, *12*, 2103050. [[CrossRef](#)]
3. Patel, D.; Robinson, J.B.; Ball, S.; Brett, D.J.L.; Shearing, P.R. Thermal Runaway of a Li-Ion Battery Studied by Combined ARC and Multi-Length Scale X-ray CT. *J. Electrochem. Soc.* **2020**, *167*, 090511. [[CrossRef](#)]
4. Liao, Z.; Zhang, S.; Li, K.; Zhao, M.; Qiu, Z.; Han, D.; Zhang, G.; Habetler, T.G. Hazard analysis of thermally abused lithium-ion batteries at different state of charges. *J. Energy Storage* **2020**, *27*, 101065. [[CrossRef](#)]
5. Yang, Y.; Fang, D.; Maleki, A.; Kohzadi, S.; Liu, Y.; Chen, Y.; Liu, R.; Gao, G.; Zhi, J. Characterization of Thermal-Runaway Particles from Lithium Nickel Manganese Cobalt Oxide Batteries and Their Biotoxicity Analysis. *Accts Appl. Energy Mater.* **2021**, *4*, 10713–10720. [[CrossRef](#)]
6. Zou, K.; He, K.; Lu, S. Venting composition and rate of large-format LiNi0.8Co0.1Mn0.1O2 pouch power battery during thermal runaway. *Int. J. Heat Mass Transf.* **2022**, *195*, 123133. [[CrossRef](#)]
7. Lai, X.; Yao, J.; Jin, C.; Feng, X.; Wang, H.; Xu, C.; Zheng, Y. A Review of Lithium-Ion Battery Failure Hazards: Test Standards, Accident Analysis, and Safety Suggestions. *Batteries* **2022**, *8*, 248. [[CrossRef](#)]
8. Lebedeva, N.; Leite Patrao, R.; Lazareanu, M.; Pfrang, A.; Da Costa Barata, R. JRC’s thermal runaway propagation test campaign at pack and vehicle level. In Proceedings of the 24th GTR EVS Meeting, Online Event, 8–10 June 2022.
9. Doan, D.R. Arc Flash Calculations for Exposures to DC Systems. *IEEE Trans. Ind. Appl.* **2010**, *46*, 2299–2302. [[CrossRef](#)]
10. Xiong, R.; Ma, S.; Li, H.; Sun, F.; Li, J. Toward a Safer Battery Management System: A Critical Review on Diagnosis and Prognosis of Battery Short Circuit. *iScience* **2020**, *23*, 101010. [[CrossRef](#)] [[PubMed](#)]
11. Abaza, A.; Ferrari, S.; Wong, H.K.; Lyness, C.; Moore, A.; Weaving, J.; Blanco-Martin, M.; Dashwood, R.; Bhagat, R. Experimental study of internal and external short circuits of commercial automotive pouch lithium-ion cells. *J. Energy Storage* **2018**, *16*, 211–217. [[CrossRef](#)]
12. Rheinfeld, A.; Noel, A.; Wilhelm, J.; Kriston, A.; Pfrang, A.; Jossen, A. Quasi-Isothermal External Short Circuit Tests Applied to Lithium-Ion Cells: Part I. Measurements. *J. Electrochem. Soc.* **2018**, *165*, A3427. [[CrossRef](#)]
13. Yang, R.; Xiong, R.; Shen, W. Experimental Study on External Short Circuit and Overcharge of Lithium-ion Battery Packs for Electric Vehicles. In Proceedings of the 2020 4th International Conference on Green Energy and Applications (ICGEA), Singapore, 7–9 March 2020; pp. 1–6. [[CrossRef](#)]
14. Fu, Y.; Zhang, P.; Verboncoeur, J.; Wang, X. Electrical breakdown from macro to micro/nano scales: A tutorial and a review of the state of the art. *Plasma Res. Express* **2020**, *2*, 013001. [[CrossRef](#)]
15. Ledinki, T.; Golubkov, A.; Schweighofer, O.; Erker, S. *Arcing in Li-Ion Batteries: Supplementary Information*; TU Graz: Graz, Austria, 2023. [[CrossRef](#)]
16. Golubkov, A.W.; Scheikl, S.; Planteu, R.; Voitic, G.; Wiltsche, H.; Stangl, C.; Fauler, G.; Thaler, A.; Hacker, V. Thermal runaway of commercial 18650 Li-ion batteries with LFP and NCA cathodes – impact of state of charge and overcharge. *RSC Adv.* **2015**, *5*, 57171–57186. [[CrossRef](#)]
17. Zhao, H.; Li, X.; Jia, S.; Murphy, A.B. Prediction of the critical reduced electric field strength for carbon dioxide and its mixtures with 50% O₂ and 50% H₂ from Boltzmann analysis for gas temperatures up to 3500 K at atmospheric pressure. *J. Phys. D Appl. Phys.* **2014**, *47*, 325203. [[CrossRef](#)]
18. Lehr, J.; Ron, P. Electrical Breakdown in Gases. In *Foundations of Pulsed Power Technology*; John Wiley & Sons, Ltd: Hoboken, NJ, USA, 2017; pp. 369–438. [[CrossRef](#)]
19. Nybeck, C.N.; Wetz, D.A.; Dodson, D.A.; Heinzel, J.M. Investigation of the Dielectric Breakdown Strength of Vented Li-Ion Electrolyte. *IEEE Trans. Plasma Sci.* **2018**, *46*, 3438–3443. [[CrossRef](#)]

Disclaimer/Publisher’s Note: The statements, opinions and data contained in all publications are solely those of the individual author(s) and contributor(s) and not of MDPI and/or the editor(s). MDPI and/or the editor(s) disclaim responsibility for any injury to people or property resulting from any ideas, methods, instructions or products referred to in the content.